Nucleoredoxin regulates WNT signaling during pituitary stem cell differentiation.

Michelle L. Brinkmeier[1], Leonard Y. M. Cheung[1,3], Sean P. O'Connell[2], Diana K. Gutierrez[2], Eve C. Rhoads[1], Sally A. Camper[1], Shannon W. Davis*[2]

[1]Department of Human Genetics, University of Michigan, Ann Arbor, MI, 48109-5618, USA.
[2]Department of Biological Sciences, University of South Carolina, Columbia, SC, 29208, USA.
[3]Current address: Department of Physiology and Biophysics, Renaissance School of Medicine, State University of New York, Stonybrook, NY 11794, USA

*Corresponding author
Department of Biological Sciences, University of South Carolina, 715 Sumter St., Columbia, SC 29208, USA.

author emails and orcid:
Brinkmeier: rollerm@umich.edu, 0000-0001-9505-4682
Cheung: leonard.cheung@stonybrook.edu, 0000-0002-0912-9594
O'Connell: soconnell@tutanota.com, 0009-0002-1161-5337
Gutierrez : dianakg@email.sc.edu, 0009-0000-7650-8722
Rhoads: ec01rhoa@siena.edu
Camper: scamper@umich.edu, 0000-0001-8556-3379
Davis: swdavis@mailbox.sc.edu, 0000-0001-7354-5691

key words
red-ox, WNT signaling, SOX2, growth hormone, cleft palate, Robinow syndrome, scRNAseq

Highlights

- *Nxn* deficiency causes neonatal lethality, cleft palate, craniofacial abnormalities, and other structural birth defects.
- *Nxn* deficiency causes pituitary dysmorphology.
- Analysis of scRNA seq reveals delayed trajectory during early pituitary cell differentiation.
- *Nxn* deficiency reduces canonical and non-canonical Wnt signaling in developing pituitary glands.
- *Nxn* deficiency reduces stem cell differentiation into pituitary hormone-producing cells.

Abstract

Nucleoredoxin (*Nxn*) encodes a multi-functional enzyme with oxidoreductase activity that regulates many different signaling pathways and cellular processes in a redox-dependent manner. Rare *NXN* mutations are reported in individuals with recessive Robinow syndrome, which involves mesomelic skeletal dysplasia, short stature, craniofacial dysmorphisms, and incompletely penetrant heart and palate defects. Here we report that *Nxn* is expressed in the ventral diencephalon and developing pituitary gland, and that *Nxn* deficient mice have pituitary dysmorphology and craniofacial abnormalities that include defects in the skull base and cleft palate. *Nxn* mutant mice exhibit reduced WNT signaling and reduced differentiation of pituitary stem cells into hormone-producing cells. These results suggest patients with Robinow syndrome could benefit from evaluation by endocrinologists for pituitary structural imaging and hormone insufficiency.

Introduction

Nucleoredoxin function and human disease

Maintenance of reduction-oxidation equilibrium is important to protect cells from oxidant damage and to initiate damage repair [1]. Nucleoredoxin (NXN) is a thioredoxin that can regulate cellular redox homeostasis [2,3]. NXN interacts with multiple proteins to regulate several pathways. These include disheveled (DVL), protein phosphatase (PP2A), phosphofructokinase (PFK1), endoplasmic reticulum transport protein (SEC63), regulator of interleukin and Toll-like receptor signaling (MYD88), regulation of actin polymerization (FLII), and calcium, calmodulin dependent protein kinase **(**CAMK2A) [4]. DVL integrates WNT signals through both the canonical WNT-β-catenin and non-canonical WNT-planar cell polarity (PCP) pathways. NXN acts as a redox sensor; in the presence of reactive oxygen species, its cysteine residues are reduced, which results in release of disheveled [3]. This can result in reduced or increased WNT signaling [5,6].

Biallelic mutations in *NXN* are a rare cause of Robinow Syndrome, which is characterized by short stature, skeletal dysplasia that includes mesomelic limb shortening, and mild facial dysmorphology [7-9]. Some Robinow syndrome cases are associated with cleft lip and/or cleft palate [10]. Robinow syndrome can also be caused by mutations in other genes that are important in the WNT/PCP signaling pathway, including *WNT5A,* the disheveled genes *DVL1, DVL2,* and *DVL3,* and the WNT co-receptors *FZD2* and *ROR2* [8,9]. Like *NXN,* bi-allelic loss of function mutations in the *WNT5A* co-receptor *ROR2* causes Robinow syndrome, while mutations in the other causative genes are dominant. Carboxy-terminal, dominant negative mutations in *DVL* genes account for most cases to date (~33%), and missense mutations in *WNT5A* and *FZD2* each account for about 9.5% of cases.

Role of WNT signaling in pituitary, hypothalamic, and palate development

WNT signaling is required for many aspects of pituitary development: 1) the expansion of Rathke's pouch, which is the primordium for the anterior (pars distalis) and intermediate lobes (pars intermedia) of the pituitary gland [11-13], 2) the development of the posterior lobe (pars nervosa) and pituitary stalk, which is surrounded by the pars tuberalis [14,15], 3) postnatal expansion of the pituitary gland [16], and 4) pituitary remodeling in mature animals [17,18]. It is also important for patterning and differentiation in the hypothalamus, especially the neurons that regulate anterior pituitary function [19]. Finally, both canonical and noncanonical WNT signaling are necessary for normal palate development [6]. Activation of WNT signaling in pituitary stem cells during development can cause adamantinomatous craniopharyngioma in mice and

humans [20,21]. WNT signaling may contribute to hypothalamic hamartoma, early onset, non-progressive pituitary adenoma, and both functioning and non-functioning symptomatic pituitary adenomas [22-25].

The mechanisms whereby WNT signaling affects pituitary growth in normal and disease states are beginning to emerge. Early studies demonstrated roles for *Wnt4, Wnt5a,* and *Wnt11* [13,26,27]. Pinpointing the role of individual WNT genes in pituitary development has been challenging because there are 19 WNT genes in mammals, and at least 14 of them are expressed in pituitary gland [16,28,29]. However, recent studies have elegantly demonstrated that pituitary stem cells expressing SOX2 secrete WNTs to stimulate nearby lineage-committed progenitors to proliferate during the postnatal period of pituitary growth [16].

Many transcription factors that are critical for hypothalamic and/or pituitary development are regulated by β-catenin, and disruption of these genes can affect pituitary development and/or function, including TCF7L1, TCF7L2, PROP1, POU1F1, PITX2, LEF1, NR5A1, FOXO1, and FOXO3 [29-41]. In addition, SOX2 and SOX3 can suppress WNT signaling [42], and mutations in these genes also cause hypopituitarism [24,43].

Nucleoredoxin and hypopituitarism

Mutations in approximately 90 genes can cause hypopituitarism [44,45], but many cases do not yet have mutations in known genes. We identified 50 genes that cause pituitary developmental abnormalities in embryonic lethal or sub-viable mouse knockouts that have not previously been associated with pituitary abnormalities [44]. We hypothesized that some of these genes could be associated with syndromic hypopituitarism in humans. We discovered that mice homozygous for nucleoredoxin (*Nxn*) loss-of-function have anterior pituitary dysmorphology, and we show here that the differentiation of stem cells to hormone producing cells is reduced. These results are important because they reveal a role for NXN in pituitary development and suggest that individuals with biallelic *NXN* mutations may benefit from endocrine evaluation.

Materials and methods

Mice

All procedures using mice were approved by the University of Michigan Committee on Use and Care of Animals, and all experiments were conducted in accordance with the principles and procedures outlined in the National Institutes of Health Guidelines of the Care and Use of Experimental Animals.

Nxn$^{em1(IMPC)J}$ mice were generated at the Jackson Lab by CRISPR/Cas gene editing in the C57BL/6N genetic background. They contain a 5 bp deletion of ATCGC in exon 2 beginning at Chromosome 11 negative strand position 76278553bp (GRCm38). This mutation is predicted to cause amino acid sequence changes after residue 133 and early truncation 21 amino acids later: p.Ser134fsAsnTer155. Sperm from this strain were purchased from Mutant Mouse Resource and Research Center at University of California, Davis (RRID:MMRRC_048884-UCD). In vitro fertilization was performed by The University of Michigan Transgenic Animal Model Core facility using eggs from female C57BL/6NJ donors (RRID:IMSR_JAX:005304). Founder mice were mated with C57BL/6J (RRID:IMSR_JAX:000664).

Mice were maintained at the University of Michigan through heterozygous crosses. All mice were housed in a 12-hour light, 12-hour dark cycle in ventilated cages with unlimited access to tap water and Purina 5020 chow. The morning after conception is designated e0.5 and the day of birth is designated as P0.

Genotyping

Genomic DNA was amplified by PCR in separate reactions for the wild type and mutant alleles. The forward oligonucleotides for the wild type (5' AGTCTCCAACATTCCATCGC 3') and mutant alleles (5' ACCGAGTCTCCAACATTCCT 3') were amplified with the reverse oligonucleotide primer (5' AGTGTTGGTAGCTGGGTTCT 3') under the following conditions: 92 C 2 min followed by 30 cycles of: 90 C 10 sec, 57 C 30 sec, 72 C 30 sec, and a final hold at 4 C. The wild type and mutant alleles produced 378 and 377 bp bands, respectively.

Single cell RNA sequencing (scRNAseq)

We dissected pituitary glands from control (1 wild type, 1 heterozygote) and 2 *Nxn* mutants at e14.5 and dispersed the pooled tissue to single cells in 50µl of a solution containing 1mg/ml papain (Roche, cat# 10108014001), 5mM L-cysteine, 1mM EDTA, and 0.6mM 2-mercaptoethanol. Dissociation was performed at 37°C for 5 minutes, with titration every 2 minutes. The samples were neutralized in 75µl of Neurobasal Media (Invitrogen, cat# 12348017) with 10% fetal bovine serum (Corning, cat# MT35010CV). The single cells were treated with 0.75µl of RNAse free Recombinant DNase I (Roche, cat#4716728001) at 37°C for 5 minutes. Single cells were pelleted in a pre-chilled microfuge for 5 minutes at 300 RCF. The supernatant was aspirated, and the cells were resuspended in 50µl Neurobasal Media with 1% fetal bovine serum. Cell viability was analyzed using the Countess 3 cell counter (Invitrogen). Viability was excellent: 95% for control and 90% for mutant. Samples were processed to create cDNA libraries at the University of Michigan Advanced Genomics Core according to a standard pipeline [46] using the 10x Genomics Chromium platform and controller, following the

manufacturer's instructions for Single Cell 3' v3 reagents, and sequenced on the NovaSeq6000 platform with an S4 chip. Sequencing reads were processed, and cells were clustered using Seurat 4.1.0. For controls and mutants, respectively, the number of cells sequenced was 19,625 and 15,918, the mean reads/cell was 27,387 and 34,783, and median genes/cell was 911 and 777. Single-cell RNA sequencing (scRNAseq) data described here are available on the National Center for Biotechnology Information Gene Expression Omnibus [47] using accession numbers GSM8628052 and GSE281783. The control pool was reported previously, GSM7864907 and GSE246211 [44].

Immunohistochemistry and in situ hybridization

Immunostaining was carried out on tissues fixed in paraformaldehyde, embedded in paraffin, and sectioned and stained as previously described [48]. Antibody sources, dilutions and detection methods are listed in **Supplementary Material, Table 1**.

RNAscope in situ hybridization for *Nxn* (Cat # 507321) was performed as previously described, including the RNAscope 2.5 HD Brown Detection kit, from Advanced Cell Diagnostics (Cat#322360).

Skeletal staining

Skeletal preparations were stained with alcian blue and alizarin red to visualize cartilage and bone, respectively [49]. The areas of cartilage and bone staining were calculated with Image J2, Fiji [50].

Statistical Analysis

We used Prism-GraphPad to create graphs and compute statistics for cell number. Data are presented as standard error of the mean (SEM) and evaluated with Student's unpaired t test or multiple unpaired t test.

Results

Nucleoredoxin mutations and pituitary dysmorphology

NXN encodes a 435 amino acid protein that is conserved in vertebrates and is 98% identical in mice (Chr 11) and humans (Chr 17). It contains a thioredoxin fold that catalyzes disulfide bond formation and isomerization (**Figure 1A**). Five loss-of-function variants have been reported in humans [8,9,51]. Mouse *Nxn* knockouts and a hypomorphic (reduced function) allele have been reported, although the pituitary gland and hypothalamus have not been examined (**Supplemental Figure 1**) [1,52-56]. We characterized the *Nxn*$^{em1(IMPC)J}$ allele, which we refer to here as *Nxn*$^{-/-}$. It contains a 5 bp deletion, c.479del483 (NM_008750), which is predicted to produce a truncated protein, p.Ser134fsAsnTer155 that would lack functional domains. We intercrossed *Nxn*$^{+/-}$ mice and obtained a normal distribution of genotypes at e10.5-e11.5 (N=76, p=0.11), e14.5 (N=118, p=0.99), and e17.5-e18.5 (N=82, p=0.19), but no mutants at 2-3 wk (N=116, p = 0.001). (**Supplemental Table 2)**. Other *Nxn* loss of function alleles are lethal at birth, and a hypomorphic allele *Nxn*^{11Jus13} exhibited reduced viability by weaning [1,52,53]. The lethality has been attributed to heart and palate defects, while the placenta is normal.

Nxn is expressed broadly [2], and we detected it in cDNA libraries from pituitaries collected at e12.5 and e14.5 [29]. We used RNAscope in situ hybridization to characterize the spatial and temporal expression of *Nxn* during pituitary and hypothalamic development (**Figure 1B**). Expression was detected in Rathke's pouch, the precursor of the anterior and intermediate lobes of the pituitary gland, and in the ventral diencephalon and developing infundibulum at e11.5 and e12.5. At e14.5-e17.5 expression persisted in the ventral diencephalon and posterior lobe, but expression in the anterior lobe was strong in the marginal zone or stem cell niche, and weak in the cells beginning to differentiate (located more ventrally and rostrally than the stem cells).

Histological analysis of *Nxn*$^{-/-}$ embryos revealed dysmorphology of Rathke's pouch from e11.5 through e17.5 (**Figure 1C**). At 11.5 the mutant pouch was thin and poorly developed. At e12.5 the dorsal aspect of the pouch was highly dysmorphic, suggesting over-proliferation of the stem cell niche and/or failure of progenitors to delaminate and move into the parenchyma of the developing anterior lobe. The dysmorphology we noted in mutants at e14.5 was like the mutant embryos presented in the Deciphering the Mechanisms of Developmental Disorders (DMDD) database using high-resolution episcopic microscopy (HREM) images [44,57,58]. The developing posterior lobe appeared smaller than normal.

Craniofacial abnormalities and fully penetrant cleft palate in *Nxn* mutants

We collected *Nxn* $^{-/-}$ mutants at e18.5 and noted variable penetrance of facial clefting and micro-ophthalmia or anophthalmia (**Supplemental Fig. 2**). We visually inspected the palate and noted completely penetrant cleft palate in mutants (N=7/7; and 6/7 were severe). To quantify alterations in craniofacial structures we prepared skeletons from e18.5 embryos with alizarin red and alcian blue staining (**Fig. 2A-F**). No abnormalities were noted in wild type (N=4) or *Nxn*$^{+/-}$ heterozygous embryos (N=16), but the homozygous mutants (*Nxn* $^{-/-}$) had fully penetrant craniofacial defects and incomplete ossification of the basisphenoid bone within the skull base (100%, N=7). The length of the head, nasal bone, and mandible were all significantly shorter in mutants (**Fig. 2G)**. We quantified the relative size of the opening in the basisphenoid bone to the area of the entire bone, and we found that the size of the opening was variable in mutants, but on average it was ~8x larger in mutants (5.6% $\pm$ 0.02) than wild type or heterozygotes (0.06 $\pm$ 0.01%).

scRNAseq analysis of gene expression

To assess the effect of *Nxn* deficiency on gene expression in the pituitary gland we conducted scRNAseq on control and mutant pools of cells from dissected pituitaries of e14.5 fetuses. 15 cell clusters were identified in controls and mutants (**Figure 3A**). We used our knowledge of cell-type specific markers to define the clusters (**Supplemental Fig. 3**) [15,46,59]. In general, the pituitary cell clusters associated with Rathke's pouch are defined by transcripts for *Epcam* (**Fig. 3B**) [60], and the transcription factors *Lhx3, Pitx1, Prop1, Pou1f1, Gata2* and *Tbx19* (**Fig. 3C**). The neural clusters are defined by transcripts for the transcription factors *Rax* and *Nkx2.1*, and the absence of *Epcam1* expression.

As expected, *Nxn* transcripts were broadly detected in controls, but not in mutants (**Fig. 4A**). The clusters with the highest levels of *Nxn* expression in Rathke's pouch were *Sox2* expressing stem cells, *Prop1* expressing progenitors, and intermediate lobe progenitors. *Nxn* transcripts were also abundant in the ventral diencephalon, infundibulum, and surrounding mesenchyme. Direct effects of *Nxn* deficiency on gene expression would be expected in these cell types. Little or no *Nxn* transcripts were detected in the corticotropes, committed *Pou1f1* cells, or rostral tip thyrotropes (pars tuberalis), which are derived from Rathke's pouch and surround the pituitary stalk [15]. This is consistent with the results of the *Nxn* in situ hybridization.

Nxn deficient mice have altered WNT signaling in the infundibulum and anterior pituitary gland

Mutations in *WNT5A* are one cause of Robinow syndrome, and *Wnt5a* mutant mice have dysmorphic pituitary glands with early alterations in BMP and FGF signaling [13,26,51]. *Wnt5a*

is expressed in the infundibulum and at lower levels in the *Sox2* expressing progenitors in Rathke's pouch (**Fig. 4**). Little or no *Wnt5a* transcripts were detected in either of these clusters in mutants. TCF7L2 function is activated by β-catenin, and *Tcf7l2* deficiency stimulates pituitary growth [31]. *Tcf7l2* is expressed in the mesenchyme, vasculature, infundibulum, and several cell types in Rathke's pouch, including stem cells, *Prop1* expressing progenitors, and intermediate lobe progenitors. Controls and mutants had similar levels of *Tcf7l2* transcripts in the infundibulum, but *Tcf7l2* transcripts were reduced in the other cell types in the mutants. In addition, *Nxn* deficiency did not affect *Fgf8* transcripts in the infundibulum. Thus, *Nxn* deficiency reduces *Wnt5a* expression in the infundibulum and *Tcf7l2* expression in Rathke's pouch-derived cells.

<u>*Nxn* deficiency affects the proportions of Rathke's pouch derived cell types</u>

We re-clustered the scRNA seq data using *Epcam1* expression to focus on Rathke's pouch-derived cell types [60]. We detected nine distinct clusters. At e14.5 there are *Sox2* expressing stem cells within the pars distalis that will give rise to cells that express ACTH, GH, TSH, the gonadotropins LH and FSH, and PRL [61]. At this stage intermediate lobe progenitors still express *Sox2,* and they have not yet activated detectable expression of *Pax7* or *Pomc.* However, they are distinguished from the other stem cells by higher expression of *Vax1* and *Npy* (**Fig. 5.**). We detected two clusters of progenitor cells expressing *Prop1* (a, b) and two expressing *Pou1f1* (a, b). We detected pars distalis thyrotropes expressing *Pou1f1, Cga,* and *Tshb.* We also detected the *Pou1f1*-independent rostral tip thyrotropes, and corticotropes. *Gh, Prl, Nr5a1, Lhb,* and *Fshb* transcripts were not detected at this age[62]. We compared the cell types between control and mutants and identified significant changes in the number of cells in some, but not all cell types (**Fig. 6A**). For example, the *Sox2* expressing progenitors and intermediate lobe progenitors are similar in number between the two genotypes. However, the *Prop1* a cluster, expressing *Aldh1a2* and *Ccne1,* was more abundant in mutants (28.2%) than controls (15.2%). The abundance of the *Pou1f1* a cluster was also elevated in mutants (29.4%) relative to controls (8.4%). In contrast, the clusters designated as *Prop1* b*, Pou1f1* b, pars distalis thyrotropes, and rostral tip thyrotropes were less abundant in mutants than controls [*Prop1* b, 6.5% (M), 10.7% (C); *Pou1f1* b, 2.1% (M), 19.9% (C); pars distalis thyrotropes 5.3% (M), 7.2% (C); rostral tip thyrotropes, 5.8% (M), 14.6% (C)]. Because *Nxn* is more strongly expressed in the progenitors than in more differentiated cells like rostral tip thyrotropes and *Pou1f1* expressing cells, the skewing of cell proportions in mutants relative to controls suggests

that the *Nxn* deficiency is slowing the progression of progenitors to more differentiated cell fates of the rostral tip thyrotrope and *Pou1f1* lineages.

We used pseudotime software to predict the trajectory of *Sox2*-expressing stem cells, which are highly proliferative at e14.5, into differentiating cells that have exited the cell cycle and exhibit reduced expression of *Mik67* (**Fig. 6B**). The pseudotime trajectory is consistent with expectations based on spatial and temporal expression of cell type specific markers. *Sox2*-expressing pituitary stem cells give rise to intermediate lobe progenitors that differentiate into *Pomc*-expressing cells later in development. The *Sox2*-expressing cells also progress to express *Prop1,* and later commit to the *Pou1f1* lineage, which is just emerging at e14.5 [34,63]. Some pars distalis thyrotropes are detectable by *Tshb* and *Pou1f1* transcripts at e14.5. Later in development the *Pou1f1* cells will differentiate into cells producing GH (somatotropes) and PRL (lactotropes). The first cell types to differentiate in pituitary development are the rostral tip thyrotropes, defined by expression of *Gata2* and *Tshb,* but not *Pou1f1.* These cells are readily identifiable and map at a distance from the stem cell cluster (**Fig. 6B**). Corticotropes, defined by *Tbx19* and *Pomc* expression, are also present at e14.5 and map far from the stem cell cluster.

There was a clear, genotypic difference in pseudotime values when the UMAP was split by genotype (**Fig. 6C**). We plotted pseudotime by density (scaled cell numbers), which reveals 3-4 distinct peaks. The peak representing the root, *Sox2*-expressing progenitors, is similar between genotypes, but the mutants have more cells in mid-trajectory and far fewer cells towards the end of the trajectory. Thus, pseudotime analysis reveals the paucity of more differentiated cells in mutants relative to controls. The scRNA sequencing data was also analyzed with TIME-CoExpress, a novel bioinformatic approach, which also detected a reduction in WNT signaling and a delayed differentiation of progenitor cells [64].

<u>Validation of *Nxn*-dependent changes in gene expression in pituitary tissue</u>

To validate findings from scRNA seq analysis we examined expression of *Sox2, Pou1f1,* and *Lef1* in control and mutant tissue at e14.5 (**Fig. 7**). As expected, *Sox2* is expressed in the ventral diencephalon, infundibulum, and the marginal (stem cell) zone of the pituitary at e14.5. The marginal zone is dysmorphic and enlarged in mutants. Immunostaining generally revealed reduced POU1F1 and LEF1 staining in mutants relative to controls. All mutants had pituitary dysmorphology, but some had less profound reduction in POU1F1 and LEF1 immunostaining relative to controls. We stained for TSHB at e15.5 because the protein is not readily detected at e14.5, and we detected a reduction in the number of pars distalis thyrotropes (*Pou1f1*-dependent) in mutants (7%) compared to controls (10%), $p<0.01$. Thus, the changes in mRNA

transcripts detected by scRNAseq e14.5 are reflected by the immunohistochemical staining in intact tissue at e14.5-e15.5.

Hormone and vasculature development appear unaffected in *Nxn* mutants

We examined pituitary development at e18.5 to determine whether the *Nxn* deficiency affected differentiation of anterior lobe hormone producing cell types that were not yet differentiated at e14.5. Histological staining revealed persistent dysmorphology of the marginal zone in mutants at e18.5 (**Supplementary Figure 4**). Immunostaining was carried out for the gonadotrope marker NR5A1, and the hormones GH, TSH and POMC. While there were no obvious differences in the pattern of immunostaining for hormones, the dysmorphic region contained cells expressing GH, TSH, and POMC. There were no obvious differences in the vasculature, as visualized by immunostaining for PECAM (**Supplementary Figure 5**).

Conclusions

Nxn deficiency causes neonatal lethality, cleft palate, craniofacial abnormalities, heart defects, eye defects, and reduction in overall growth in mice [5,52,53] (**Supplemental Table 3).** The underlying mechanisms involve NXN-mediated effects on the pool of DVL protein [5]. Binding of NXN to DVL prevents its interaction with other proteins, including KLHL12, a ubiquitin ligase that marks DVL for degradation [5]. The results of *Nxn* deficiency vary by tissue. For example, the skeletal defects in *Nxn* mutants are associated with hyperactivated WNT-β-catenin signaling in osteoblasts, while the heart defects, including ventral septal defects and persistent truncus arteriosus, are associated with suppression of WNT signaling [5]. These different effects likely result from tissue-specific differences in the pool of DVL.

We discovered pituitary dysmorphology in developing *Nxn* mutant embryos at e14.5 [44]. The role of *Nxn* in pituitary-hypothalamic development had not been investigated. Here we report *Nxn* gene expression during pituitary development, and the effect of *Nxn* deficiency in $Nxn^{em1(IMPC)J}$ homozygous mice ($Nxn^{-/-}$) at the earliest stages of pituitary development, including reduction in pituitary cell differentiation and reduced expression of key regulatory genes. Genes encoding members of both the canonical and non-canonical WNT signaling pathways were reduced in pituitary development. We also confirm and extend the effects of *Nxn* deficiency on other structures.

$Nxn^{-/-}$ exhibit embryonic lethality. Their craniofacial defects include significant shortening of head length, mandible, and nasal bone, like the $Nxn^{tm1Hmik}$ null homozygotes [1]. Cleft palate, anophthalmia and microphthalmia, have been reported in *Nxn* deficient mice (**Supplemental**

Table 3). The cleft palate in *Nxn*$^{-/-}$ embryos was 100% penetrant, and the majority (89%) had a complete cleft. In addition, we identified a cranial base fenestra in the basisphenoid bone. The basisphenoid bone, along with the pituitary, is a midline structure sensitive to SHH signaling [65,66]. Inhibition of SHH signaling is sufficient to cause a fenestra in the basisphenoid bone. The basisphenoid fenestra in *Nxn*$^{-/-}$ embryos suggests that WNT signaling may also contribute to basisphenoid formation, possibly by inhibiting SHH signaling [67]. In support of this idea, *Ptch1* and *Gli3* expression is reduced in the *Nxn* mutant pituitary progenitor cells.

Nxn is expressed in both the developing posterior lobe and Rathke's pouch, and these structures were affected in *Nxn*$^{-/-}$ homozygotes. The developing posterior lobe was smaller and had reduced expression of *Wnt5a. Wnt5a* typically acts non-canonically through the WNT/Ca2+ and WNT/planar cell polarity (PCP) pathways, and it can antagonize canonical WNT signaling [68]. *Nxn* deficiency caused abnormalities in Rathke's pouch from the onset of invagination through late gestation, especially the marginal zone where progenitors reside. This dysmorphology bears some similarity to that observed in *Wnt5a*$^{-/-}$ embryos [13,26]. The caudal side of the pouch appears smaller in both *Nxn*$^{-/-}$ and *Wnt5a*$^{-/-}$ embryos. However, the rostral side is not expanded in *Nxn*$^{-/-}$ like *Wnt5a*$^{-/-}$ embryos. A reduction in the length of the caudal side of Rathke's pouch is also caused by decreased SHH signaling [65]. Because the e11.5 *Nxn*$^{-/-}$ embryos do not have the rostral expansion of pituitary progenitors, it seems unlikely that the dysmorphology observed at e12.5 and e14.5 is caused by changes in the pituitary signaling center seen in *Wnt5a*$^{-/-}$ embryos, i.e. expansion of BMP and FGF signaling [13]. Consistent with this, we observed reduced *Wnt5a* expression in the infundibulum, but no changes in *Fgf8* or *Fgf10* expression. Thus, *Nxn* deficiency reduces non-canonical WNT signaling in the developing posterior lobe of the pituitary gland, and the planar cell polarity pathway is important for pituitary development [69].

The scRNA sequencing technology provides a powerful tool for phenotyping mutant embryos, and for generating hypotheses about the role of the mutant gene in normal development [59,70]. We used scRNA sequencing to assess changes in pituitary cell populations and identify gene expression changes at e14.5 in *Nxn* mutants, and we found that *Nxn* delays pituitary progenitor cell differentiation. There are excellent markers for pituitary cell types after birth [46,71], but many of these are not expressed until later in gestation. We used pseudotime analysis to map the differentiation of cell types from *Sox2* expressing precursor cells. We identified cells at each stage in the developmental trajectory along with their transcriptional profile. SOX2+ stem cells transition to PROP1+ progenitor cells (*Prop1* a) that begin expression of *Pou1f1* (*Prop1* b). Each of these cell types normally express *Nxn.* The *Pou1f1* progenitors

(*Pou1f1* a) have reduced *Prop1* expression and increased *Pou3f4* transcripts. They progress to a cell type the expresses *Neurod4* (*Pou1f1* b). Loss of *Nxn* delays the transition from *Prop1* a to *Prop1* b progenitors. Cells that do progress are delayed at the *Pou1f1* a progenitor stage. *Nxn*$^{-/-}$ embryos have decreased expression of *Lef1* and *Pou1f1* at the RNA and protein levels. PROP1, LEF1, and POU1F1 interact with β-catenin to regulate transcription [32,33]; therefore, the delayed differentiation at each stage is likely caused by reduced canonical WNT signaling.

All individuals reported with Robinow syndrome and *NXN* variants appear to have biallelic loss of function alleles (**Supplemental Table 4**) [9,51]. They all exhibit craniofacial abnormalities, skeletal dysplasia including mesomelia, and brachydactyly. They differ in presentation of cleft palate, even between siblings. A *NXN* patient homozygous for p.Arg209* had GH deficiency, but it is not clear whether the other patients were assessed for an endocrine contribution to their short stature. The delay in pituitary development that we observed in *Nxn*-deficient mice may underlie the short stature in some patients. The homozygous *Nxn* mice die at birth, which is attributable to their heart and palate defects [5,52]. The individual homozygous for *NXN* p.Arg209* had a heart defect, as well as kidney anomalies, omphalocele, and two ventral hernias which were not reported in other patients. Thus, some babies with *NXN* biallelic loss of function alleles may not be viable. The variation in phenotypic features might be due to genetic background and environmental factors [72].

This study benefited from the phenotypic analysis conducted by the centers associated with the IMPC and the ready availability of cryopreserved null alleles of *Nxn* generated by the knockout mouse project. These resources enabled an in-depth phenotyping of pituitary gland organogenesis in *Nxn*$^{-/-}$ embryos, providing a plausible explanation for the endocrine deficiency observed in an individual with Robinow syndrome. Endocrine assessment of other children with Robinow syndrome could identify those who could benefit from hormone replacement therapy. Finally, analysis of other embryonic lethal strains with pituitary dysmorphology will enrich our understanding of the etiology of pituitary dysfunction in humans [44].

Acknowledgements

Funding for this work was from University of South Carolina, University of Michigan, and the National Institutes of Health (R01 HD108156 to SAC and SWD, and R01HD097096 to SAC). We thank the Transgenic Animal Model and Advanced Genomics Core facilities at University of Michigan for rederiving the mice and performing single cell sequencing. We thank Drs. Prasov, Mishina, Pérez-Millán, Ellsworth, and Raetzman for useful comments.

References

1 Funato, Y. & Miki, H. Redox regulation of Wnt signalling via nucleoredoxin. *Free Radic Res* **44**, 379-388, doi:10.3109/10715761003610745 (2010).

2 Kurooka, H. *et al.* Cloning and characterization of the nucleoredoxin gene that encodes a novel nuclear protein related to thioredoxin. *Genomics* **39**, 331-339, doi:10.1006/geno.1996.4493 (1997).

3 Funato, Y., Michiue, T., Asashima, M. & Miki, H. The thioredoxin-related redox-regulating protein nucleoredoxin inhibits Wnt-beta-catenin signalling through dishevelled. *Nat Cell Biol* **8**, 501-508, doi:10.1038/ncb1405 (2006).

4 Idelfonso-Garcia, O. G. *et al.* Is Nucleoredoxin a Master Regulator of Cellular Redox Homeostasis? Its Implication in Different Pathologies. *Antioxidants (Basel)* **11**, doi:10.3390/antiox11040670 (2022).

5 Funato, Y. *et al.* Nucleoredoxin sustains Wnt/beta-catenin signaling by retaining a pool of inactive dishevelled protein. *Curr Biol* **20**, 1945-1952, doi:10.1016/j.cub.2010.09.065 (2010).

6 Zhang, Z., Pan, X., Chen, M. & Bai, M. Wnt signalling in oral and maxillofacial diseases. *Cell Biol Int* **46**, 34-45, doi:10.1002/cbin.11708 (2022).

7 McPherson, E., Zaleski, C. & Giampietro, P. F. Robinow syndrome with variable neurologic features. *Genet Med* **8**, 59-60, doi:10.1097/01.gim.0000195294.57969.92 (2006).

8 Zhang, C. *et al.* Novel pathogenic variants and quantitative phenotypic analyses of Robinow syndrome: WNT signaling perturbation and phenotypic variability. *HGG Adv* **3**, 100074, doi:10.1016/j.xhgg.2021.100074 (2022).

9 Zhang, C. *et al.* Novel pathogenic genomic variants leading to autosomal dominant and recessive Robinow syndrome. *Am J Med Genet A* **185**, 3593-3600, doi:10.1002/ajmg.a.61908 (2021).

10 Shprintzen, R. J., Goldberg, R. B., Saenger, P. & Sidoti, E. J. Male-to-male transmission of Robinow's syndrome. Its occurrence in association with cleft lip and cleft palate. *Am J Dis Child* **136**, 594-597, doi:10.1001/archpedi.1982.03970430026007 (1982).

11 Osmundsen, A. M., Keisler, J. L., Taketo, M. M. & Davis, S. W. Canonical WNT Signaling Regulates the Pituitary Organizer and Pituitary Gland Formation. *Endocrinology* **158**, 3339-3353, doi:10.1210/en.2017-00581 (2017).

12 Youngblood, J. L., Coleman, T. F. & Davis, S. W. Regulation of Pituitary Progenitor Differentiation by beta-Catenin. *Endocrinology* **159**, 3287-3305, doi:10.1210/en.2018-00563 (2018).

13 Potok, M. A. *et al.* WNT signaling affects gene expression in the ventral diencephalon and pituitary gland growth. *Dev Dyn* **237**, 1006-1020, doi:10.1002/dvdy.21511 (2008).

14 Voutetakis, A. Pituitary stalk interruption syndrome. *Handb Clin Neurol* **181**, 9-27, doi:10.1016/B978-0-12-820683-6.00002-6 (2021).

15 Cheung, L. Y. M. *et al.* Novel Candidate Regulators and Developmental Trajectory of Pituitary Thyrotropes. *Endocrinology* **164**, doi:10.1210/endocr/bqad076 (2023).

16 Russell, J. P. *et al.* Pituitary stem cells produce paracrine WNT signals to control the expansion of their descendant progenitor cells. *Elife* **10**, doi:10.7554/eLife.59142 (2021).
17 Gremeaux, L., Fu, Q., Chen, J. & Vankelecom, H. Activated phenotype of the pituitary stem/progenitor cell compartment during the early-postnatal maturation phase of the gland. *Stem Cells Dev* **21**, 801-813, doi:10.1089/scd.2011.0496 (2012).
18 Willems, C. *et al.* Regeneration in the Pituitary After Cell-Ablation Injury: Time-Related Aspects and Molecular Analysis. *Endocrinology* **157**, 705-721, doi:10.1210/en.2015-1741 (2016).
19 Newman, E. A., Wu, D., Taketo, M. M., Zhang, J. & Blackshaw, S. Canonical Wnt signaling regulates patterning, differentiation and nucleogenesis in mouse hypothalamus and prethalamus. *Dev Biol* **442**, 236-248, doi:10.1016/j.ydbio.2018.07.021 (2018).
20 Gaston-Massuet, C. *et al.* Increased Wingless (Wnt) signaling in pituitary progenitor/stem cells gives rise to pituitary tumors in mice and humans. *Proc Natl Acad Sci U S A* **108**, 11482-11487, doi:10.1073/pnas.1101553108 (2011).
21 Andoniadou, C. L. *et al.* Sox2(+) stem/progenitor cells in the adult mouse pituitary support organ homeostasis and have tumor-inducing potential. *Cell Stem Cell* **13**, 433-445, doi:10.1016/j.stem.2013.07.004 (2013).
22 Alatzoglou, K. S. *et al.* SOX2 haploinsufficiency is associated with slow progressing hypothalamo-pituitary tumours. *Hum Mutat* **32**, 1376-1380, doi:10.1002/humu.21606 (2011).
23 Kelberman, D. *et al.* SOX2 plays a critical role in the pituitary, forebrain, and eye during human embryonic development. *J Clin Endocrinol Metab* **93**, 1865-1873, doi:10.1210/jc.2007-2337 (2008).
24 Kelberman, D. *et al.* Mutations within Sox2/SOX2 are associated with abnormalities in the hypothalamo-pituitary-gonadal axis in mice and humans. *J Clin Invest* **116**, 2442-2455, doi:10.1172/JCI28658 (2006).
25 Elston, M. S. *et al.* Wnt pathway inhibitors are strongly down-regulated in pituitary tumors. *Endocrinology* **149**, 1235-1242, doi:10.1210/en.2007-0542 (2008).
26 Cha, K. B. *et al.* WNT5A signaling affects pituitary gland shape. *Mech Dev* **121**, 183-194, doi:10.1016/j.mod.2003.12.002 (2004).
27 Kerr, J. M. *et al.* Growth arrest of thyrotropic tumors by thyroid hormone is correlated with novel changes in Wnt-10A. *Mol Cell Endocrinol* **238**, 57-67, doi:10.1016/j.mce.2005.03.004 (2005).
28 Nusse, R. & Clevers, H. Wnt/beta-Catenin Signaling, Disease, and Emerging Therapeutic Modalities. *Cell* **169**, 985-999, doi:10.1016/j.cell.2017.05.016 (2017).
29 Brinkmeier, M. L. *et al.* Discovery of transcriptional regulators and signaling pathways in the developing pituitary gland by bioinformatic and genomic approaches. *Genomics* **93**, 449-460, doi:10.1016/j.ygeno.2008.11.010 (2009).
30 Gaston-Massuet, C. *et al.* Transcription factor 7-like 1 is involved in hypothalamo-pituitary axis development in mice and humans. *Proc Natl Acad Sci U S A* **113**, E548-557, doi:10.1073/pnas.1503346113 (2016).
31 Brinkmeier, M. L., Potok, M. A., Davis, S. W. & Camper, S. A. TCF4 deficiency expands ventral diencephalon signaling and increases induction of pituitary progenitors. *Dev Biol* **311**, 396-407, doi:10.1016/j.ydbio.2007.08.046 (2007).

32 Olson, L. E. *et al.* Homeodomain-mediated beta-catenin-dependent switching events dictate cell-lineage determination. *Cell* **125**, 593-605, doi:10.1016/j.cell.2006.02.046 (2006).
33 Skowronska-Krawczyk, D. *et al.* Required enhancer-matrin-3 network interactions for a homeodomain transcription program. *Nature* **514**, 257-261, doi:10.1038/nature13573 (2014).
34 Sornson, M. W. *et al.* Pituitary lineage determination by the Prophet of Pit-1 homeodomain factor defective in Ames dwarfism. *Nature* **384**, 327-333, doi:10.1038/384327a0 (1996).
35 Wu, W. *et al.* Mutations in PROP1 cause familial combined pituitary hormone deficiency. *Nat Genet* **18**, 147-149, doi:10.1038/ng0298-147 (1998).
36 Li, S. *et al.* Dwarf locus mutants lacking three pituitary cell types result from mutations in the POU-domain gene pit-1. *Nature* **347**, 528-533, doi:10.1038/347528a0 (1990).
37 Tatsumi, K. *et al.* Cretinism with combined hormone deficiency caused by a mutation in the PIT1 gene. *Nat Genet* **1**, 56-58, doi:10.1038/ng0492-56 (1992).
38 Kioussi, C. *et al.* Identification of a Wnt/Dvl/beta-Catenin --> Pitx2 pathway mediating cell-type-specific proliferation during development. *Cell* **111**, 673-685, doi:10.1016/s0092-8674(02)01084-x (2002).
39 Ai, D. *et al.* Nuclear factor 1 and T-cell factor/LEF recognition elements regulate Pitx2 transcription in pituitary development. *Mol Cell Biol* **27**, 5765-5775, doi:10.1128/MCB.01848-06 (2007).
40 Parakh, T. N. *et al.* Follicle-stimulating hormone/cAMP regulation of aromatase gene expression requires beta-catenin. *Proc Natl Acad Sci U S A* **103**, 12435-12440, doi:10.1073/pnas.0603006103 (2006).
41 Stallings, C. E., Kapali, J., Evans, B. W., McGee, S. R. & Ellsworth, B. S. FOXO Transcription Factors Are Required for Normal Somatotrope Function and Growth. *Endocrinology* **163**, doi:10.1210/endocr/bqab263 (2022).
42 Wong, J., Farlie, P., Holbert, S., Lockhart, P. & Thomas, P. Q. Polyalanine expansion mutations in the X-linked hypopituitarism gene SOX3 result in aggresome formation and impaired transactivation. *Front Biosci* **12**, 2085-2095, doi:10.2741/2213 (2007).
43 Laumonnier, F. *et al.* Transcription factor SOX3 is involved in X-linked mental retardation with growth hormone deficiency. *Am J Hum Genet* **71**, 1450-1455, doi:10.1086/344661 (2002).
44 Martinez-Mayer, J. *et al.* Knockout mice with pituitary malformations help identify human cases of hypopituitarism. *Genome Med* **16**, 75, doi:10.1186/s13073-024-01347-y (2024).
45 Vishnopolska, S. A. *et al.* Comprehensive Identification of Pathogenic Gene Variants in Patients With Neuroendocrine Disorders. *J Clin Endocrinol Metab* **106**, 1956-1976, doi:10.1210/clinem/dgab177 (2021).
46 Cheung, L. Y. M. *et al.* Single-Cell RNA Sequencing Reveals Novel Markers of Male Pituitary Stem Cells and Hormone-Producing Cell Types. *Endocrinology* **159**, 3910-3924, doi:10.1210/en.2018-00750 (2018).

47 Edgar, R., Domrachev, M. & Lash, A. E. Gene Expression Omnibus: NCBI gene expression and hybridization array data repository. *Nucleic Acids Res* **30**, 207-210, doi:10.1093/nar/30.1.207 (2002).
48 Bando, H. *et al.* Heterozygous variants in SIX3 and POU1F1 cause pituitary hormone deficiency in mouse and man. *Hum Mol Genet* **32**, 367-385, doi:10.1093/hmg/ddac192 (2023).
49 Rigueur, D. & Lyons, K. M. Whole-mount skeletal staining. *Methods Mol Biol* **1130**, 113-121, doi:10.1007/978-1-62703-989-5_9 (2014).
50 Schindelin, J. *et al.* Fiji: an open-source platform for biological-image analysis. *Nature Methods* **9**, 676-682, doi:10.1038/nmeth.2019 (2012).
51 White, J. J. *et al.* WNT Signaling Perturbations Underlie the Genetic Heterogeneity of Robinow Syndrome. *Am J Hum Genet* **102**, 27-43, doi:10.1016/j.ajhg.2017.10.002 (2018).
52 Boles, M. K. *et al.* Discovery of candidate disease genes in ENU-induced mouse mutants by large-scale sequencing, including a splice-site mutation in nucleoredoxin. *PLoS Genet* **5**, e1000759, doi:10.1371/journal.pgen.1000759 (2009).
53 Perez-Garcia, V. *et al.* Placentation defects are highly prevalent in embryonic lethal mouse mutants. *Nature* **555**, 463-468, doi:10.1038/nature26002 (2018).
54 Tran, B. N. *et al.* Reduced exploratory behavior in neuronal nucleoredoxin knockout mice. *Redox Biol* **45**, 102054, doi:10.1016/j.redox.2021.102054 (2021).
55 Albrecht, N. E. *et al.* Rapid and Integrative Discovery of Retina Regulatory Molecules. *Cell Rep* **24**, 2506-2519, doi:10.1016/j.celrep.2018.07.090 (2018).
56 Valek, L., Tran, B. N. & Tegeder, I. Cold avoidance and heat pain hypersensitivity in neuronal nucleoredoxin knockout mice. *Free Radic Biol Med* **192**, 84-97, doi:10.1016/j.freeradbiomed.2022.09.010 (2022).
57 Wilson, R., McGuire, C., Mohun, T. & Project, D. Deciphering the mechanisms of developmental disorders: phenotype analysis of embryos from mutant mouse lines. *Nucleic Acids Res* **44**, D855-861, doi:10.1093/nar/gkv1138 (2016).
58 Mohun, T. *et al.* Deciphering the Mechanisms of Developmental Disorders (DMDD): a new programme for phenotyping embryonic lethal mice. *Dis Model Mech* **6**, 562-566, doi:10.1242/dmm.011957 (2013).
59 Masser, B. E. *et al.* Gene Misexpression in a Smoc2+ve/Sox2-Low Population in Juvenile Prop1-Mutant Pituitary Gland. *J Endocr Soc* **8**, bvae146, doi:10.1210/jendso/bvae146 (2024).
60 Kodani, Y. *et al.* EpCAM Is a Surface Marker for Enriching Anterior Pituitary Cells From Human Hypothalamic-Pituitary Organoids. *Front Endocrinol (Lausanne)* **13**, 941166, doi:10.3389/fendo.2022.941166 (2022).
61 Davis, S. W., Keisler, J. L., Perez-Millan, M. I., Schade, V. & Camper, S. A. All Hormone-Producing Cell Types of the Pituitary Intermediate and Anterior Lobes Derive From Prop1-Expressing Progenitors. *Endocrinology* **157**, 1385-1396, doi:10.1210/en.2015-1862 (2016).
62 Cushman, L. J. *et al.* Persistent Prop1 expression delays gonadotrope differentiation and enhances pituitary tumor susceptibility. *Hum Mol Genet* **10**, 1141-1153, doi:10.1093/hmg/10.11.1141 (2001).

63 Perez Millan, M. I., Brinkmeier, M. L., Mortensen, A. H. & Camper, S. A. PROP1 triggers epithelial-mesenchymal transition-like process in pituitary stem cells. *Elife* **5**, doi:10.7554/eLife.14470 (2016).
64 Yang, S. *et al.* TIME-CoExpress: Temporal Trajectory Modeling of Dynamic Gene Co-expression Patterns Using Single-Cell Transcriptomics Data. *bioRxiv*, 2025.2001.2023.634392, doi:10.1101/2025.01.23.634392 (2025).
65 Carreno, G. *et al.* Hypothalamic sonic hedgehog is required for cell specification and proliferation of LHX3/LHX4 pituitary embryonic precursors. *Development* **144**, 3289-3302, doi:10.1242/dev.153387 (2017).
66 Chen, J. *et al.* Defining the critical period of hedgehog pathway inhibitor-induced cranial base dysplasia in mice. *Dev Dyn* **250**, 527-541, doi:10.1002/dvdy.270 (2021).
67 Ding, M. & Wang, X. Antagonism between Hedgehog and Wnt signaling pathways regulates tumorigenicity. *Oncol Lett* **14**, 6327-6333, doi:10.3892/ol.2017.7030 (2017).
68 Guo, R. & Xing, Q. S. Roles of Wnt Signaling Pathway and ROR2 Receptor in Embryonic Development: An Update Review Article. *Epigenet Insights* **15**, 25168657211064232, doi:10.1177/25168657211064232 (2022).
69 Lodge, E. J., Barrell, W. B., Liu, K. J. & Andoniadou, C. L. The Fuzzy planar cell polarity protein (FUZ), necessary for primary cilium formation, is essential for pituitary development. *Journal of anatomy* **244**, 358-367, doi:10.1111/joa.13961 (2024).
70 Cheung, L. Y. M. & Camper, S. A. PROP1-Dependent Retinoic Acid Signaling Regulates Developmental Pituitary Morphogenesis and Hormone Expression. *Endocrinology* **161**, doi:10.1210/endocr/bqaa002 (2020).
71 Mayran, A. *et al.* Pioneer and nonpioneer factor cooperation drives lineage specific chromatin opening. *Nat Commun* **10**, 3807, doi:10.1038/s41467-019-11791-9 (2019).
72 Kohli, S. S. & Kohli, V. S. A comprehensive review of the genetic basis of cleft lip and palate. *J Oral Maxillofac Pathol* **16**, 64-72, doi:10.4103/0973-029X.92976 (2012).
73 Groza, T. *et al.* The International Mouse Phenotyping Consortium: comprehensive knockout phenotyping underpinning the study of human disease. *Nucleic Acids Res* **51**, D1038-d1045, doi:10.1093/nar/gkac972 (2023).

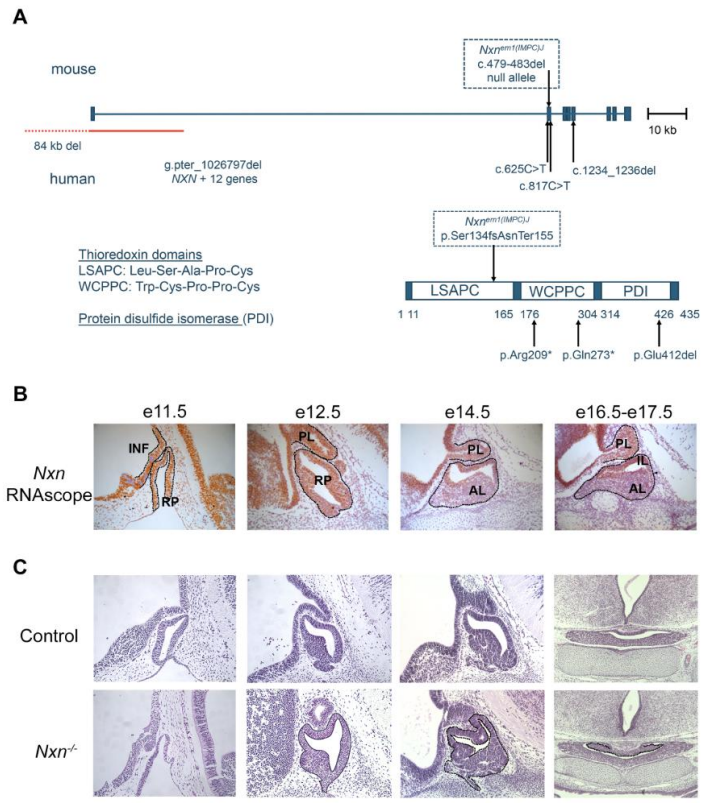

Figures and legends

Figure 1. Nucleoredoxin loss of function mutations, pituitary gene expression, and dysmorphology

A. The mouse *Nxn* gene is shown with the positions of the variants in the *Nxn*$^{em1/J}$ (referred to here as *Nxn*$^{-/-}$) allele. Clinically reported mutations in NXN are indicated below the diagram [8,9,51]. A diagram of the protein domains shows the thioredoxin domains, LSAPC (Leu-Ser-Ala-Pro-Cys) and WCPPC (Trp-Cys-Prop-Pro-Cys), and the protein disulfide isomerase domain (PDI). B. Control and *Nxn*$^{-/-}$ fetuses were collected at e11.5, e12.5, e14.5 and e16.5-e17.5. *Nxn* expression was assessed with RNAscope in situ hybridization in control tissues (orange). Transcripts were detected in the infundibulum (INF), Rathke's pouch (RP), the posterior lobe (PL), and the anterior and intermediate lobes (IL, AL respectively). C. Sections stained with eosin and hematoxolin revealed dysmorphology in Rathke's pouch tissue (black outline) in mutants at e11.5, e12.5 and e14.5 (sagittal). Dysmorphology was evident in e16.5-e17.5 sections (coronal), (black outline).

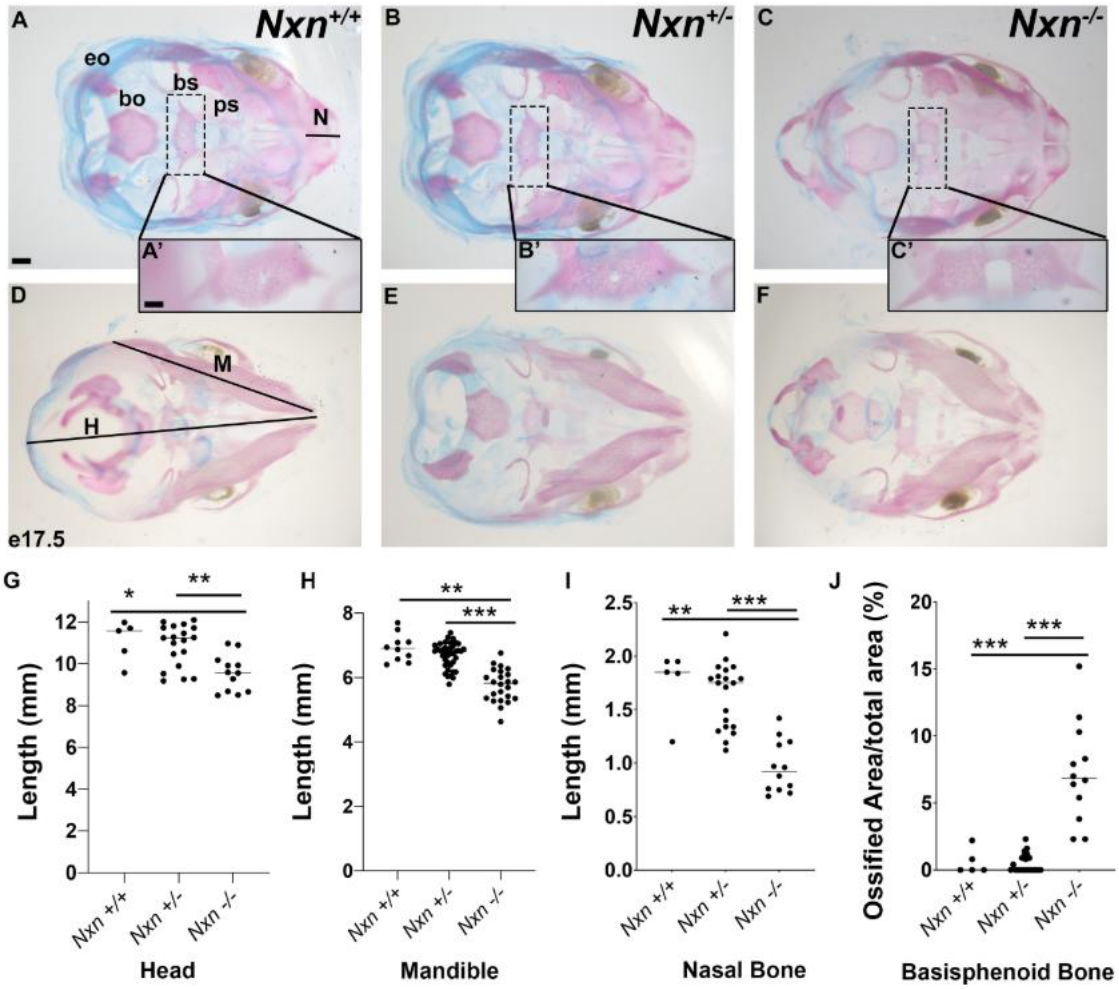

Figure 2. Nucleoredoxin deficiency causes craniofacial dysmorphology and incomplete ossification of the basisphenoid bone

Fetuses were collected at e18.5, and skeletons were prepared with alcian blue to visualize cartilage and alizarin red for bone. Preparations were photographed from dorsal (A, B, C) and ventral perspectives (D, E, F). The length of the nasal bone (N), head (H), and mandible (M) were quantified. The exoccipital (eo), basioccipital (bo), basisphenoid (bs), presphenoid (ps) bones are indicated, and the insets show an enlargement of the basisphenoid bone (A', B', C'). The basisphenoid bone was incompletely ossified in *Nxn*$^{-/-}$ embryos, and the size of the opening was measured relative to the total area of this element (G). Bone and opening measurements are indicated for fetuses collected at e18.5 of each genotype: wild type (N=4), heterozygote (N=16), and mutant (N=7). The p values are designated as *** = $p<0.01$, ** = $p<0.05$.

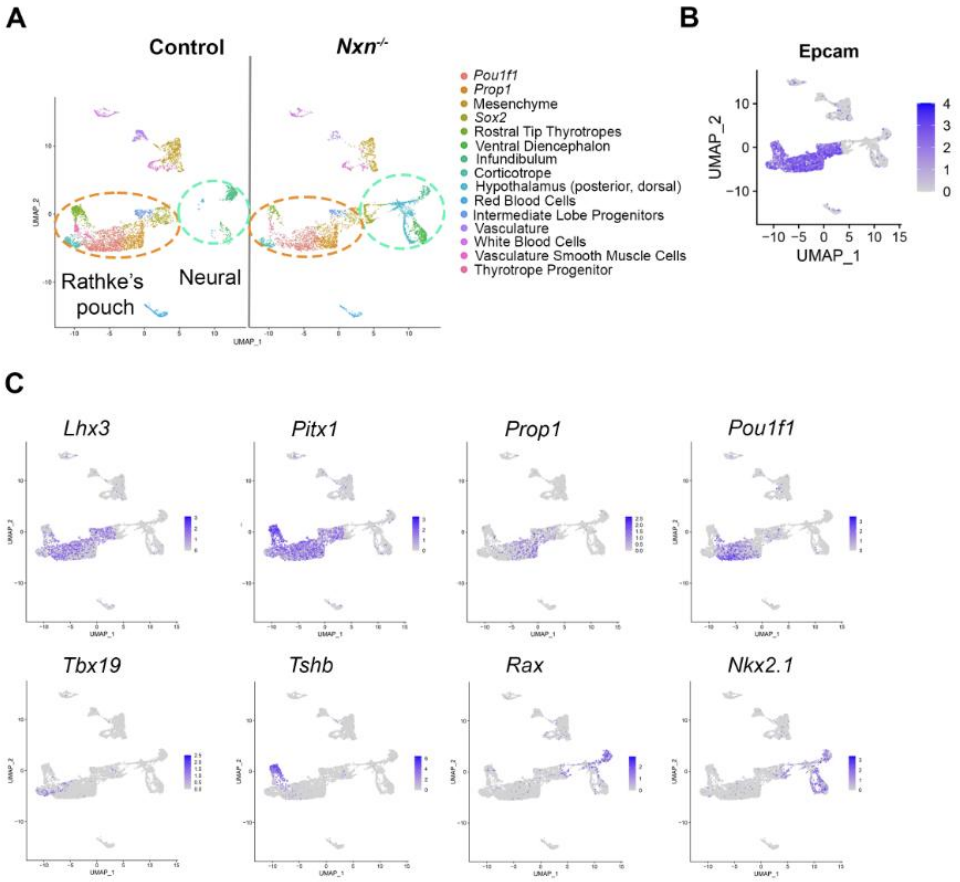

Figure 3. scRNAseq cell clusters are defined by *Epcam1*, various transcription factors and hormone gene expression.

A. UMAP plots of scRNAseq data from pituitaries collected from control and *Nxn*$^{-/-}$ fetuses at e14.5. B. UMAP plot illustrating strong *Epcam* expression in Rathke's pouch derived cell types. C. UMAP plots of lineage specific transcription factors that were used to assign cell cluster identity.

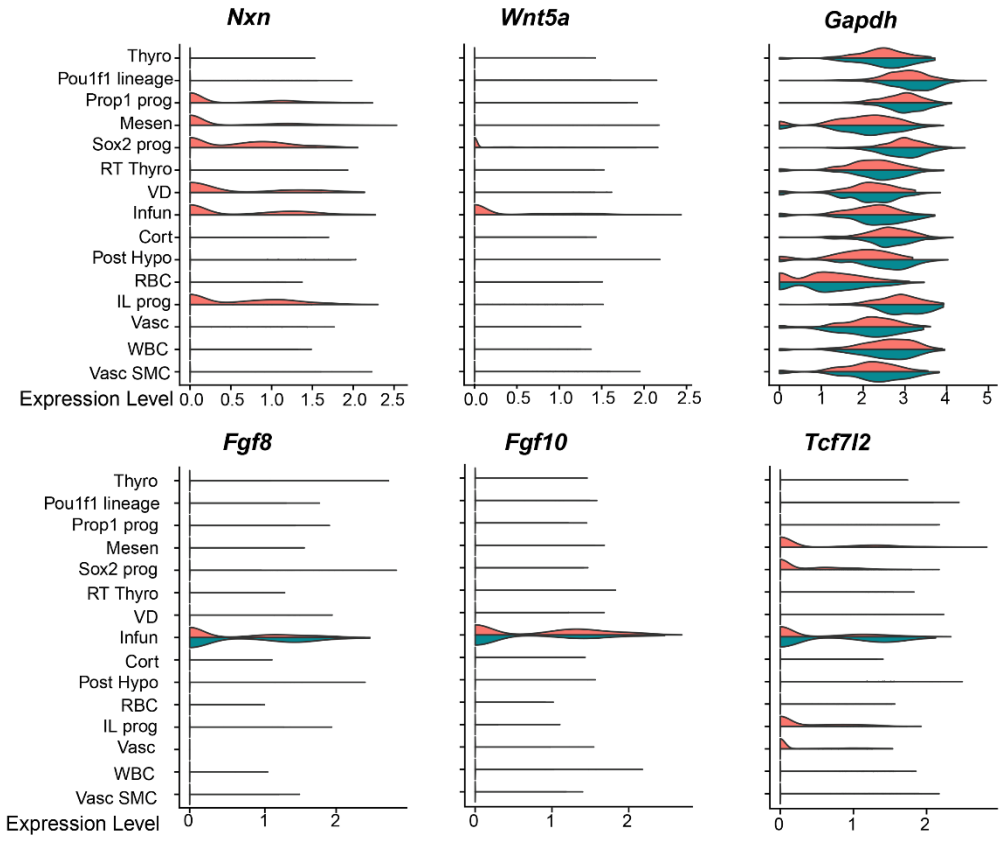

Fig. 4. Reduced non-canonical Wnt signaling in *Nxn* mutants.

Mutations in NXN or WNT5A can cause Robinow syndrome. Violin plots illustrate the detection of *Nxn* transcripts in the control scRNAseq pool (orange), but not in the mutants (green). *Nxn* transcripts are predominantly localized to the mesenchyme, neural ectoderm derived infundibulum and ventral diencephalon, and the Rathke's pouch derived cells that include *Sox2*-expressing stem cells, and *Prop1*-expressing progenitors. Violin plots indicate a reduction in *Wnt5a* gene expression in the infundibulum of *Nxn* mutants relative to littermate controls. In contrast, the β-catenin responsive gene *Tcf7l2* is equivalently expressed in the infundibulum of *Nxn* mutants and littermate controls. There were no differences in *Fgf8* or *Fgf10* expression between *Nxn* mutants and controls, and GAPDH is expressed equivalently in both groups.

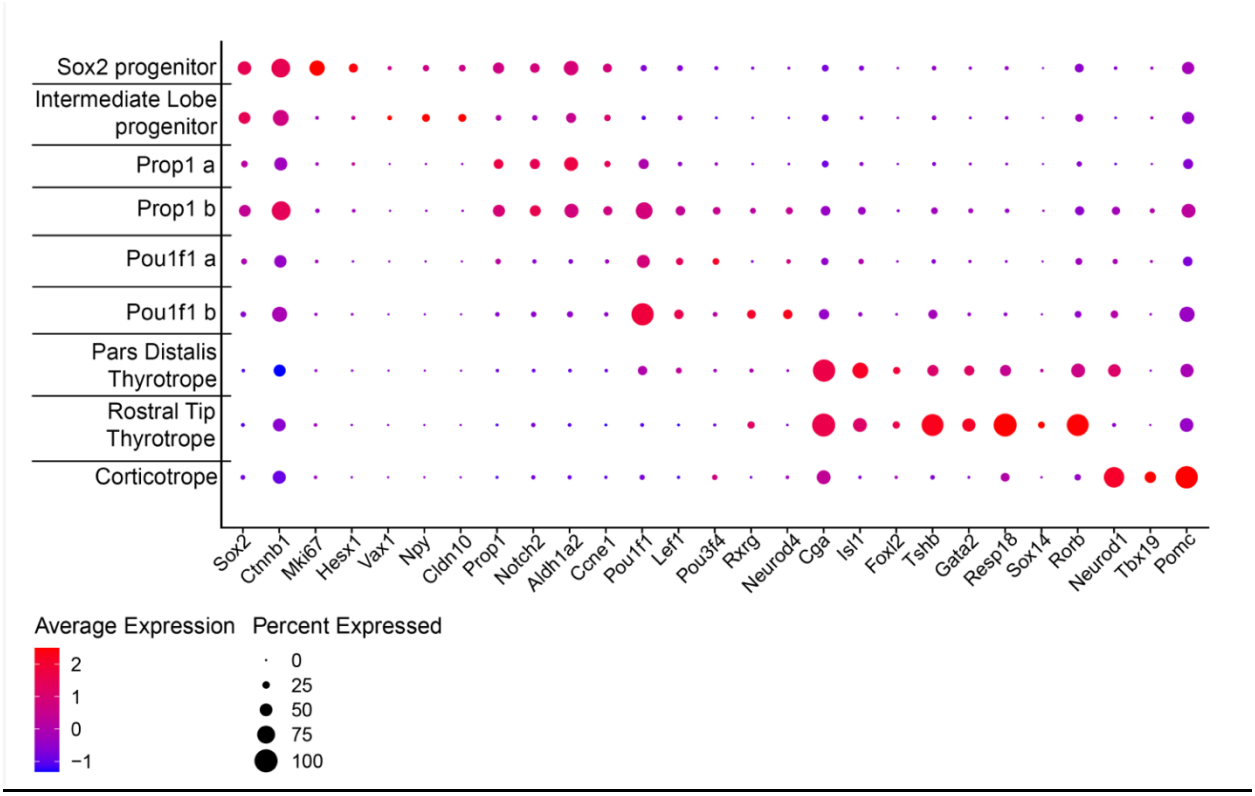

<u>Figure 5: Gene expression in Rathke's pouch derived cells defines cell clusters.</u> Rathke's pouch derived cells were identified based on *Epcam1* expression and re-clustered. Nine distinct clusters were detected. *Sox2* is expressed in stem cells that give rise to hormone producing cells in the anterior lobe (*Sox2* progenitors) and the intermediate lobe (Intermediate lobe progenitors). There are two clusters of cells with strong *Prop1* expression, (*Prop1 a* and *Prop1 b*). The *Prop1 b* cluster expresses higher levels of *Pou1f1* and markers of more differentiated cells like *Lef1, Rxrg,* and *Neurod4.* There are two clusters of *Pou1f1* expressing cells (*Pou1f1 a* and *Pou1f1 b*). The *Pou1f1 b* cluster has lower levels of *Prop1* than *Pou1f1 a.* The pars distalis thyrotropes and rostral tip thyrotropes (pars tuberalis) differ in that the former express *Pou1f1* and the latter express higher levels of *Sox14* and *Rorb.* Finally, corticotropes express *Neurod1, Tbx19, Pomc.*

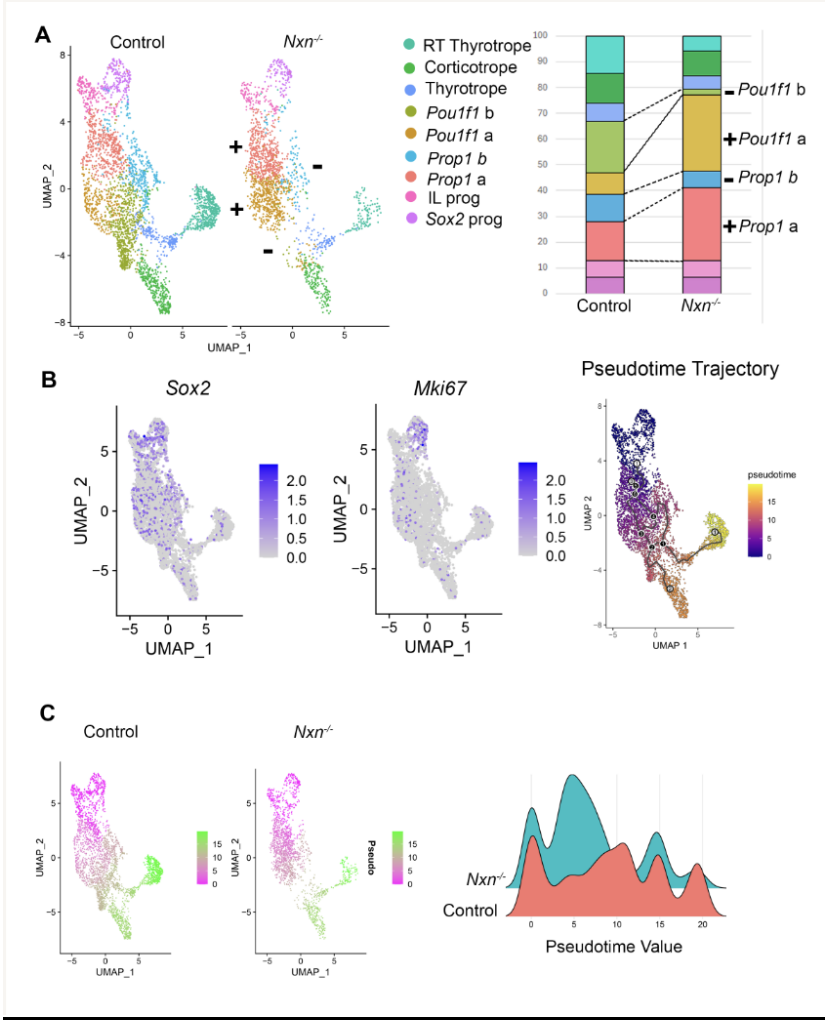

Figure 6. *Nxn* deficiency causes a reduced differentiation.

A. UMAP clustering of Rathke's pouch derived cell types from e14.5 pituitaries from controls and *Nxn* mutant littermates. Stacked bar chart indicating the fraction of cells that are in each cluster. Significant differences between controls and mutants are indicated with a + (increased in mutants relative to wild type) or - (decreased). Abbreviations: rostral tip thyrotropes (RT), intermediate lobe (IL), progenitor (prog).

B. UMAP plots indicating expression of the stem cell marker *Sox2* and the proliferation marker, *Mki67,* which provide the root for the pseudotime trajectory.

C. Pseudotime analysis UMAP plots illustrate the progression of Rathke's pouch-derived cell types from *Sox2*-expressing stem cells to differentiated cell types. The density plot compares distribution of cells along pseudotime axis.

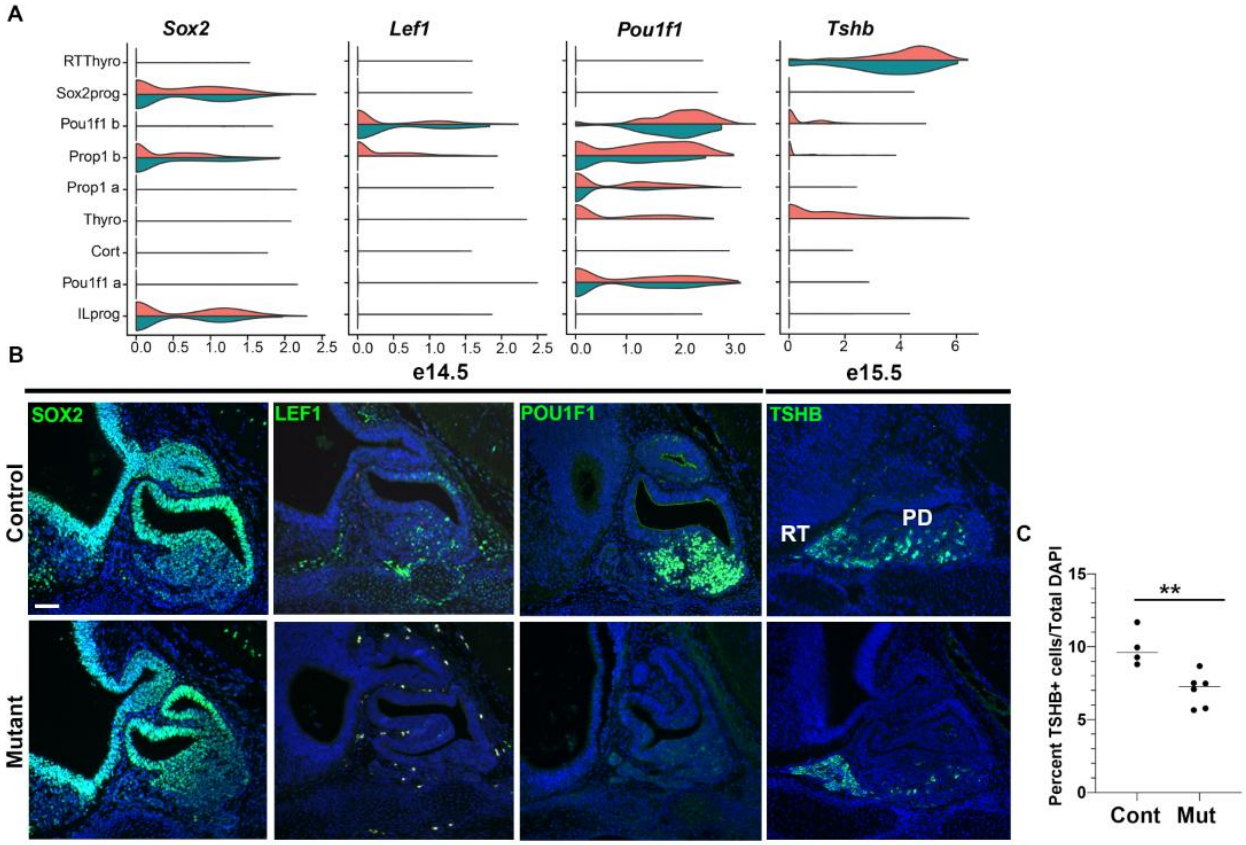

Figure 7. *Nxn* mutants have reduced expression of LEF1, POU1F1, and TSH, and fewer TSH producing cells.

A. Violin plots indicate expression levels of *Sox2, Lef1, Pou1f1,* and *Tshb* in controls (orange) and mutants (green). B. Sagittal sections from wild type (N=3) and *Nxn* $^{-/-}$ mutants (N=10) collected at e14.5 were stained with antibodies for SOX2, LEF1, and POU1F1. All mutant pituitaries exhibited dysmorphology, and 4/10 exhibited severe reduction in expression of LEF1 and POU1F1. The rostral tip thyrotropes (RT) and pars distalis thyrotropes (PD) are indicated. The scale bar= 50 uM. The p value = 0.0055 (**).

Supplementary Material

Supplementary Table 1. Antibody sources, dilutions and detection methods

Target Protein	Primary Antibody	Source	Dilution	Antigen Retrieval	Blocking	Secondary Antibody	Tertiary reagent	Detection
GH	Monkey anti-GH	National Hormone & Peptide Program, #AFP411S	1:1000	none	2%BSA, 1% normal goat serum, in 1xPBS	Goat anti-human Alexa Flour 488	none	
TSHB	Guinea pig anti-TSHb	National Hormone & Peptide Program, #AFP967793	1:500	none	2%BSA, 1% normal goat serum, in 1xPBS	Goat anti-guinea pig Alexa Fluor 488	none	
POMC	Guinea pig anti-ACTH	National Hormone & Peptide Program, #AFP71111591	1:500	none	2%BSA, 1% normal goat serum, in 1xPBS	Goat anti-guinea pig Alexa Fluor 488	none	
PECAM1	Rabbit anti-PECAM	Thermo Scientific #RB-10333	1:100	10 min boiling 0.1M Citric Acid, pH 6.0	2%BSA, 1% normal donkey serum, in 1xPBS	Donkey anti-rabbit Biotin	Strep-HRP	TSA CF488, Biotium #33002
POU1F1	Rabbit anti-POU1F1	Dr. Simon Rhodes	**1:500**	10 min boiling 0.1M Citric Acid, pH 6.0	2%BSA, 1% normal donkey serum, in 1xPBS	Donkey anti-rabbit Biotin	Strep-HRP	TSA CF488, Biotium #33002
LEF1	Goat anti-LEF1	Santa Cruz Biotechnology	1:500	10 min boiling 0.1M Citric Acid, pH 6.0	2%BSA, 1% normal donkey serum, in 1xPBS	Donkey anti-goat Biotin	Strep-HRP	TSA Alexa Fluor 488, Life Tecnologies#T20932
LHB	Guinea pig anti-LHB	National Hormone & Peptide Program	1:50	None	2%BSA, 1% normal donkey serum, in 1xPBS	Goat anti-guinea pig Alex Fluor 488	none	
NR5A1	Rabbit anti-NR5A1	custom	1:1000	10mM Citric Acid, pH 6.0	2%BSA, 1% normal donkey serum, in 1xPBS	Donkey anti-rabbit Biotin	Strep-HRP	TSA CF488, Biotium #33002

Supplemental Table 2. Mendelian distribution of *Nxn* genotypes during development

genotype	age[1]			
	e10.5-e11.5	**e14.5**	**e17.5-e18.5**	**2-3 wk**
+/+	13 (17)	11 (26)	23 (28)	30 (29)
+/-	47 (62)	21 (49)	33 (40)	86 (58)
-/-	16 (21)	11 (26)	26 (32)	0 (29)
p value	0.11	0.99	0.19	0.001**

[1]number of fetuses (percentage of total)

Supplemental Table 3. Phenotype information for homozygous and heterozygous *Nxn* alleles in mice. Multiple *Nxn* alleles have been generated and phenotyped by the International Mouse Phenotyping Consortium (IMPC) (Supplemental Fig. 1) [73]. Phenotypes for these alleles are directly deposited with Mouse Genome Informatics (MGI) (www.informatics.jax.org/) and are available for download from the IMPC website (www.mousephenotype.org).

feature	allele	genotype	gender	age	method of assessment	parameter	institution	most significant p value
abnormal mammary gland morphology	Nxn<tm1b(EUCOMM)Wtsi>	heterozygote	male	Early adult	Gross Pathology and Tissue Collection	Mammary gland	CCP-IMG	0
hemorrhage	Nxn<em1(IMPC)Mbp>	heterozygote	female	E15.5	Gross Morphology Embryo E14.5-E15.5	Hemorrhage	UC Davis	0
unresponsive to tactile stimuli	Nxn<em1(IMPC)Bay>	heterozygote	male	E18.5	Gross Morphology Embryo E18.5	Responsive to tactile stimuli	BCM	0
decreased cardiac muscle contractility	Nxn<tm1a(EUCOMM)Wtsi>	heterozygote	female	Early adult	Echo	Ejection Fraction	BCM	0.000004425057186579 11
small adrenal glands	Nxn<tm1b(EUCOMM)Wtsi>	heterozygote	male	Early adult	Gross Pathology and Tissue Collection	Adrenal gland	TCP	0
decreased body length	Nxn<em1(IMPC)Mbp>	heterozygote	female	Early adult	Organ Weight	Body length	UC Davis	0.000062575994151510 3
increased fasting circulating glucose level	Nxn<em1(IMPC)J>	heterozygote	not_considered	Early adult	Intraperitoneal glucose tolerance test (IPGTT)	Fasted blood glucose concentration	JAX	0.000007744246084850 91
increased circulating bilirubin level	Nxn<em1(IMPC)J>	heterozygote	male	Early adult	Clinical Chemistry	Total bilirubin	JAX	0.000008317155131880 09
decreased locomotor activity	Nxn<tm1b(EUCOMM)Wtsi>	heterozygote	female	Early adult	Open Field	Periphery resting time	ICS	3.78027599410494e-11
unresponsive to tactile stimuli	Nxn<tm1b(EUCOMM)Wtsi>	heterozygote	female	E18.5	Gross Morphology Embryo E18.5	Responsive to tactile stimuli	BCM	0
spina bifida	Nxn<em1(IMPC)Mbp>	heterozygote	male	E15.5	Gross Morphology Embryo E14.5-E15.5	spina bifida	UC Davis	0
abnormal behavior	Nxn<tm1a(EUCOMM)Wtsi>	heterozygote	male	Early adult	Open-field	Latency to centre entry	HMGU	0.00006443007269329
irregularly shaped pupil	Nxn<tm1a(EUCOMM)Wtsi>	heterozygote	female	Early adult	Eye Morphology	Pupil Shape	BCM	0.000018945037538594 5
abnormal digit morphology	Nxn<tm1b(EUCOMM)Wtsi>	heterozygote	male	Early adult	X-ray	Digit integrity	ICS	7.98216167332279e-7
abnormal optic disk morphology	Nxn<tm1b(EUCOMM)Wtsi>	heterozygote	not_considered	Early adult	Eye Morphology	Optic Disc	MARC	0.000013582641021189 7
abnormal cranium morphology	Nxn<tm1b(EUCOMM)Wtsi>	heterozygote	female	Early adult	X-ray	Skull shape	WTSI	0.000024098078029920 3
abnormal locomotor behavior	Nxn<tm1b(EUCOMM)Wtsi>	heterozygote	female	Early adult	Fear Conditioning	% Freezing duration habituation-1	ICS	0.000066779870017894 3
decreased exploration in new environment	Nxn<tm1b(EUCOMM)Wtsi>	heterozygote	female	Early adult	Open Field	Latency to center entry	ICS	8.73716271937624e-8
abnormal snout morphology	Nxn<tm1b(EUCOMM)Wtsi>	heterozygote	female	Early adult	Combined SHIRPA and Dysmorphology	Snout size	MRC Harwell	0.000003542886597330 35
anophthalmia	Nxn<tm1a(EUCOMM)Wtsi>	heterozygote	female	Early adult	Gross Pathology and Tissue Collection	Eye with optic nerve	BCM	0
increased grip strength	Nxn<tm1a(EUCOMM)Wtsi>	heterozygote	female	Early adult	Grip-Strength	Forelimb grip strength measurement mean	HMGU	0.000037618268205053 6
abnormal freezing behavior	Nxn<tm1b(EUCOMM)Wtsi>	heterozygote	female	Early adult	Fear Conditioning	% Freezing duration pre-cue-1	ICS	0.000012843146509548 9
abnormal eyelid morphology	Nxn<tm1b(EUCOMM)Wtsi>	heterozygote	female	Early adult	Eye Morphology	Eyelid morphology	WTSI	0.000017813517915287
increased effector memory CD8-positive, alpha-beta T cell number	Nxn<tm1b(EUCOMM)Wtsi>	heterozygote	male	Early adult	Immunophenotyping	Effector CD8+ T cells - % of live leukocytes (Panel A)	CCP-IMG	1.13003262392377e-7
increased mean corpuscular hemoglobin concentration	Nxn<em1(IMPC)J>	heterozygote	female	Early adult	Hematology	Mean cell hemoglobin concentration	JAX	0.000012796792861762 3
increased circulating triglyceride level	Nxn<tm1b(EUCOMM)Wtsi>	heterozygote	male	Early adult	Clinical Chemistry	Triglycerides	CCP-IMG	0.000046166434627015 7
short tibia	Nxn<tm1b(EUCOMM)Wtsi>	heterozygote	male	Early adult	X-ray	Tibia length	UC Davis	0.000001208959797714 198
increased circulating alkaline phosphatase level	Nxn<tm1b(EUCOMM)Wtsi>	heterozygote	female	Early adult	Clinical Chemistry	Alkaline phosphatase	ICS	0.000024986988056685 9
abnormal retina blood vessel morphology	Nxn<em1(IMPC)Bay>	heterozygote	male	Early adult	Eye Morphology	Retinal Blood Vessels Pattern	BCM	0.000006310277712698 4
increased circulating HDL cholesterol level	Nxn<tm1b(EUCOMM)Wtsi>	heterozygote	male	Early adult	Clinical Chemistry	HDL-cholesterol	CCP-IMG	0.000032073498226472 7
preweaning lethality, incomplete penetrance	Nxn<tm1a(EUCOMM)Wtsi>	homozygote	male	Early adult	Viability Primary Screen	Homozygous males viability	BCM	-
abnormal head shape	Nxn<tm1b(EUCOMM)Wtsi>	homozygote	male	E18.5	Gross Morphology Embryo E18.5	Head shape	BCM	0
abnormal embryo size	Nxn<em1(IMPC)Bay>	homozygote	male	E18.5	Gross Morphology Embryo E18.5	Embryo Size	BCM	0
abnormal facial morphology	Nxn<tm1b(EUCOMM)Wtsi>	homozygote	male	E18.5	Gross Morphology Embryo E18.5	Facial Morphology	BCM	0
cleft palate	Nxn<tm1b(EUCOMM)Wtsi>	homozygote	male	E18.5	Gross Morphology Embryo E18.5	Cleft palate	BCM	0
preweaning lethality, complete penetrance	Nxn<em1(IMPC)Mbp>	homozygote	female	Early adult	Viability Primary Screen	Homozygous females viability	UC Davis	0
abnormal facial morphology	Nxn<em1(IMPC)Bay>	homozygote	male	E18.5	Gross Morphology Embryo E18.5	Facial Morphology	BCM	0
spina bifida	Nxn<em1(IMPC)Mbp>	homozygote	female	E15.5	Gross Morphology Embryo E14.5-E15.5	spina bifida	UC Davis	0
cleft palate	Nxn<em1(IMPC)J>	homozygote	female	E18.5	Gross Morphology Embryo E18.5	Cleft palate	JAX	0
preweaning lethality, complete penetrance	Nxn<tm1b(EUCOMM)Wtsi>	homozygote	male	Early adult	Viability Primary Screen	Homozygous males viability	BCM	0
facial cleft	Nxn<tm1b(EUCOMM)Wtsi>	homozygote	female	E18.5	Gross Morphology Embryo E18.5	Facial Cleft	BCM	0
unresponsive to tactile stimuli	Nxn<tm1b(EUCOMM)Wtsi>	homozygote	female	E18.5	Gross Morphology Embryo E18.5	Responsive to tactile stimuli	BCM	0
hemorrhage	Nxn<em1(IMPC)Mbp>	homozygote	male	E15.5	Gross Morphology Embryo E14.5-E15.5	Hemorrhage	UC Davis	0
preweaning lethality, complete penetrance	Nxn<em1(IMPC)Bay>	homozygote	not_considered	Early adult	Viability Primary Screen	Homozygous animals viability	BCM	0
abnormal craniofacial morphology	Nxn<tm1b(EUCOMM)Wtsi>	homozygote	female	E12.5	Gross Morphology Embryo E12.5	Craniofacial morphology	JAX	0
cleft palate	Nxn<tm1b(EUCOMM)Wtsi>	homozygote	male	E15.5	Gross Morphology Embryo E14.5-E15.5	Cleft Palate	JAX	0
abnormal head shape	Nxn<em1(IMPC)Bay>	homozygote	male	E18.5	Gross Morphology Embryo E18.5	Head shape	BCM	0
unresponsive to tactile stimuli	Nxn<em1(IMPC)Bay>	homozygote	male	E18.5	Gross Morphology Embryo E18.5	Responsive to tactile stimuli	BCM	0
abnormal embryo size	Nxn<em1(IMPC)J>	homozygote	male	E18.5	Gross Morphology Embryo E18.5	Embryo Size	JAX	0
abnormal embryo size	Nxn<tm1b(EUCOMM)Wtsi>	homozygote	female	E18.5	Gross Morphology Embryo E18.5	Embryo Size	BCM	0
abnormal head size	Nxn<tm1b(EUCOMM)Wtsi>	homozygote	female	E18.5	Gross Morphology Embryo E18.5	Head size	BCM	0
abnormal facial morphology	Nxn<em1(IMPC)J>	homozygote	male	E18.5	Gross Morphology Embryo E18.5	Facial Morphology	JAX	0
abnormal craniofacial morphology	Nxn<tm1b(EUCOMM)Wtsi>	homozygote	no data	E15.5	Gross Morphology Embryo E14.5-E15.5	Craniofacial morphology	TCP	0
abnormal embryo size	Nxn<tm1b(EUCOMM)Wtsi>	homozygote	male	E15.5	Gross Morphology Embryo E14.5-E15.5	Embryo Size	JAX	0
facial cleft	Nxn<em1(IMPC)Bay>	homozygote	male	E18.5	Gross Morphology Embryo E18.5	Facial Cleft	BCM	0
no spontaneous movement	Nxn<tm1b(EUCOMM)Wtsi>	homozygote	no data	E18.5	Gross Morphology Embryo E18.5	Spontaneous movement	CCP-IMG	0
abnormal head size	Nxn<em1(IMPC)Bay>	homozygote	male	E18.5	Gross Morphology Embryo E18.5	Head size	BCM	0
preweaning lethality, complete penetrance	Nxn<em1(IMPC)J>	homozygote	not_considered	Early adult	Viability Primary Screen	Viability Outcome	JAX	0
facial cleft	Nxn<em1(IMPC)J>	homozygote	male	E18.5	Gross Morphology Embryo E18.5	Facial Cleft	JAX	0

Supplemental Table 4. Clinical features of individuals with *NXN* variants.

Patient identifier	inheritance	DNA	Protein	Features #	Ref
1 (8841)	homozygous	Stop gain, c.625C>T	p.Arg209*	GHD, CP, Jaw, Face, Meso, Br, He, Ki and more	[51]
2 (9844)	Compound heterozygote	In frame deletion, c.1234-1236; 84 kb deletion including exon 1 of *NXN*	p.Glu412del, none	CP, Jaw, Face, Meso, Br	[51]
3 (9847)	Compound heterozygote	Same as sister above		Jaw, Face, Meso, Br	[51]
4 (10973)	Compound heterozygote	Del17p.13.3, *NXN* and 12 other genes; nonsense, c.817C>T	None, p.Gln273*	Face, Meso, Br	[9]

# Feature code:
GHD = Growth hormone deficiency
CP = Cleft palate, absent uvula
Jaw = micrognathia
Face = facial characteristics
Meso = mesomelia
Br = brachydactyly
He = heart: bicuspid aortic valve, abnormal right coronary artery
Ki = left kidney duplication
More = omphalocele, 2x ventral hernias, ear infection, conductive HL

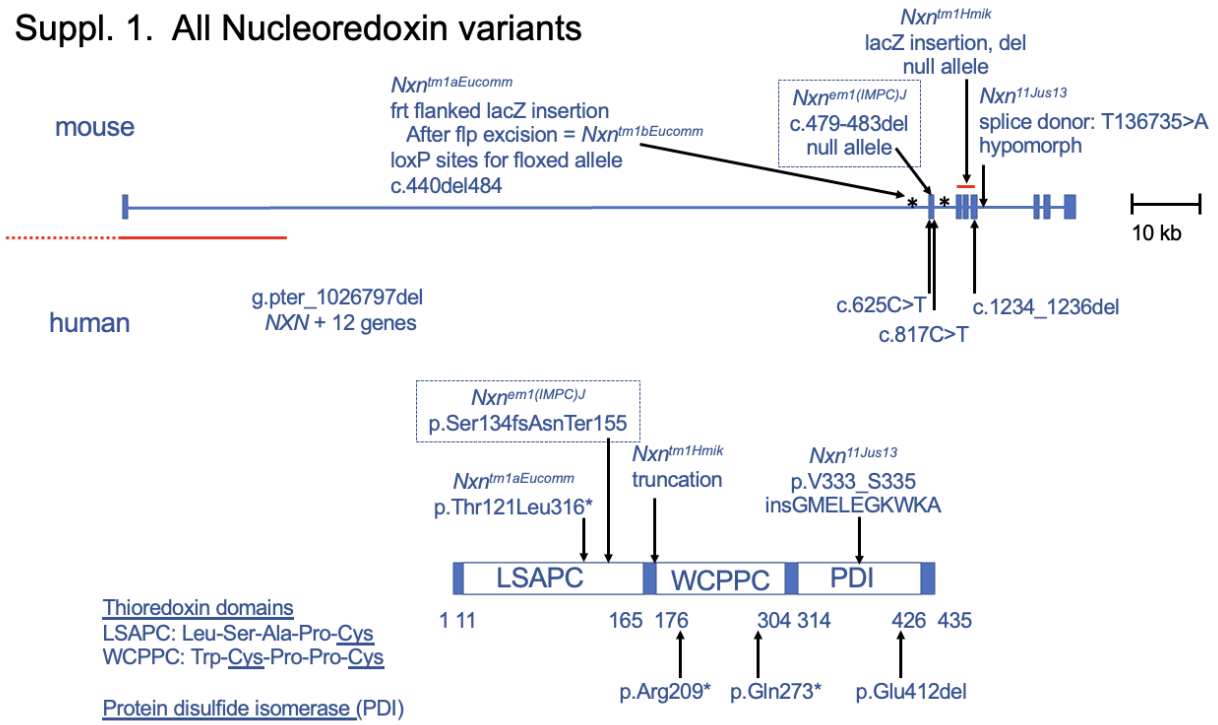

Supplemental Figure 1. Nucleoredoxin variants in mouse and man. The structure of the human and mouse nucleoredoxin genes are similar. Mouse alleles are indicated above the gene diagram, including the knockout first *Nxn*^{tm1aEucomm} allele [53], the *Nxn*$^{em1(IMPC)J}$ allele described in this manuscript, the lacZ insertion *Nxn*^{tm1Hmik} allele [1], and the hypomorphic *Nxn*^{11Jus13} allele [52]. Patient mutations in *NXN* are indicated below the gene diagram including an individual homozygous for stop gain, c.625C>T, two compound heterozygous sisters with an 84 kb deletion including exon 1 of *NXN* (red) and an in frame deletion, c.1234-1236del, and an unrelated compound heterozygote with deletion of *NXN* and 12 other genes in trans with a nonsense mutation, c.817C>T, as described [8,9,51]. The NXN protein consists of three domains indicated in the protein diagram. All variants in mouse and man are expected to be null alleles due to the loss of key protein domains, except the hypomorphic *Nxn*^{11Jus13} allele which splices normally at a low frequency.

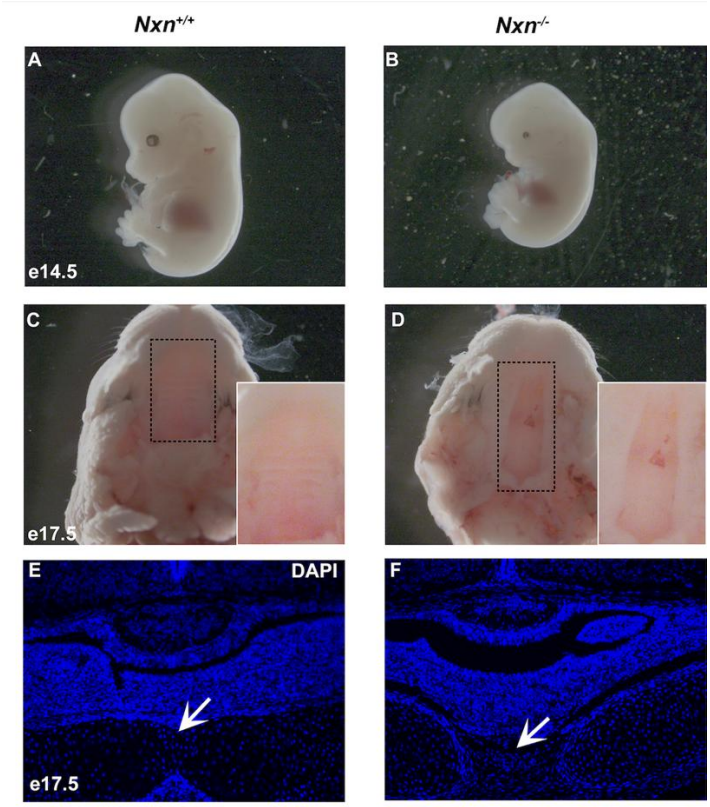

Supplemental Figure 2. Craniofacial abnormalities in *Nxn* mutants.

Wild type (A) and *Nxn* mutants (B) were collected at e14.5. None of the wild type animals had micro-ophthalmia or anophthalmia, but some of the mutants did.

Wild type (C) and mutant (D) animals were collected at e17.5, and the palates were examined. The palate area is enlarged in the inset.

Wild type (E) and mutant (F) animals were collected at e17.5, fixed, sectioned in the coronal plane, and stained with DAPI. The basisphenoid bone is fused at the base of the pituitary gland in wild type, but not mutant animals (arrows).

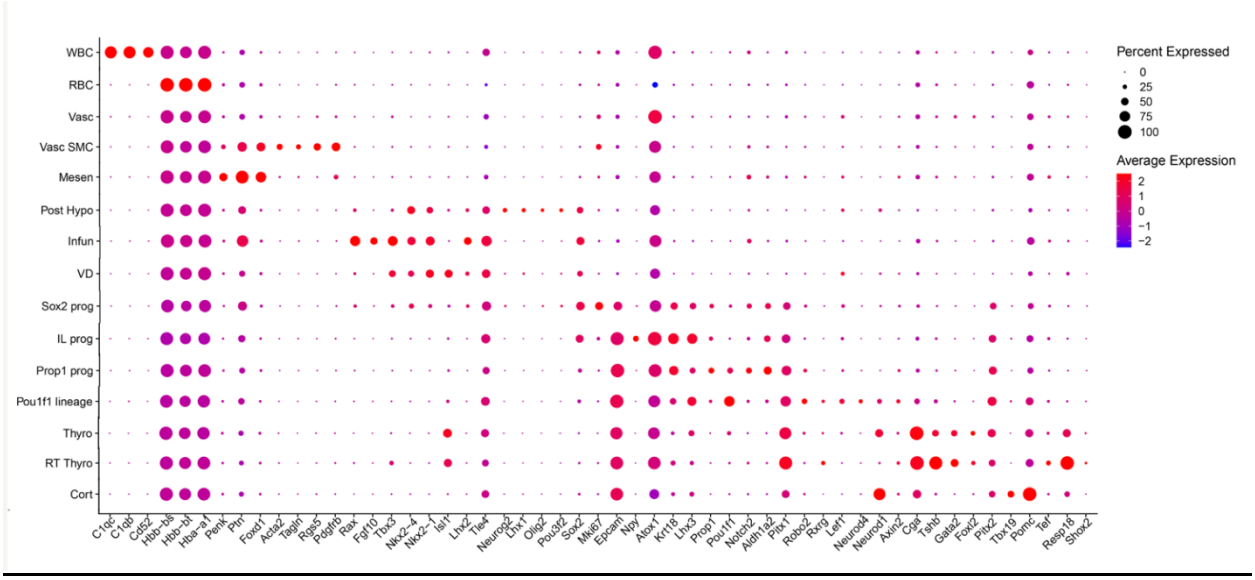

Supplemental Figure 3. Differences in gene expression associated with cell clusters.

A dot plot presents selected genes that are differentially expressed in cell clusters. Abbreviations: white blood cells (WBC), red blood cells (RBC), vasculature (Vasc), mesenchyme (Mesen), posterior hypothalamus (Post Hypo), infundibulum (Infun), ventral diencephalon (VD), progenitor (prog), intermediate lobe (IL), pars distalis thyrotrope (Thyro), rostral tip or pars tuberalis thyrotrope (RT Thyro), corticotrope (Cort).

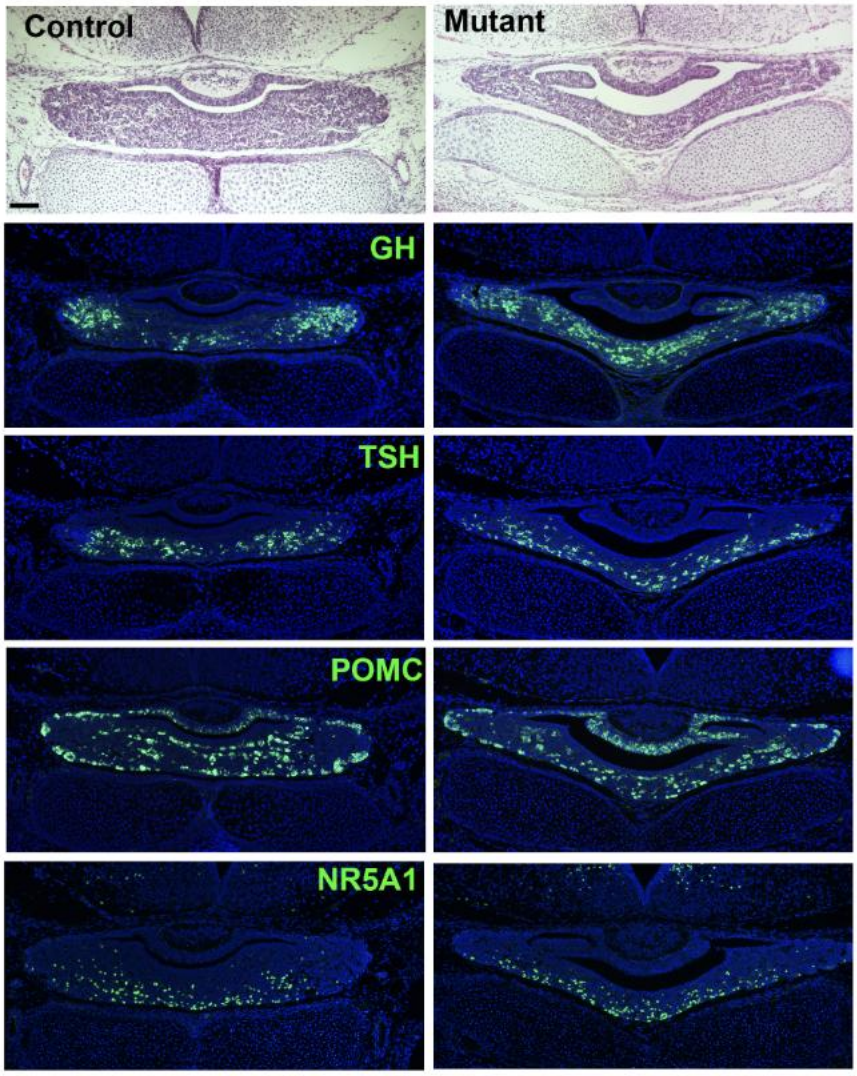

Supplemental Figure 4. Persistent dysmorphology and differentiation of gonadotrope and *Pou1f1* lineages in later development.

Pituitary glands were collected at e18.5 from controls and mutants and processed for histology by sectioning in the coronal plane. Hematoxylin and eosin staining reveals the dysmorphology that persists in the mutant pituitary. Immunostaining for NR5A1, GH, TSH and POMC did not reveal any obvious differences in mutants.

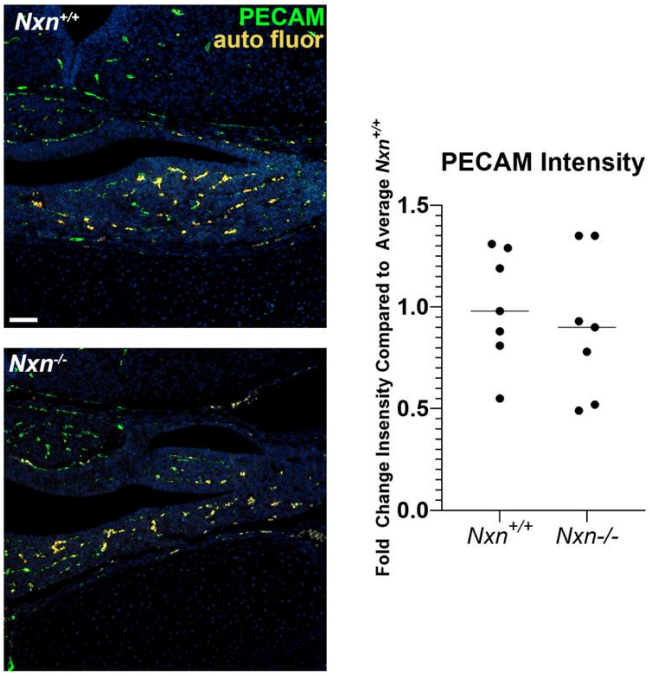

Supplementary Figure 5. *Nxn* deficiency has no obvious effect on pituitary vasculature.

A. To assess vascular development, pituitaries were collected from e18.5 wild type fetuses and *Nxn*$^{-/-}$ littermates, N=7/genotype. 2-5 coronal pituitary sections per individual were stained with PECAM1 antibodies (also known as CD31) and imaged by confocal microscopy at 20x with the green (Alexa488 laser) channel. Auto-fluorescent red blood cells were imaged with the red channel. Image J was used to quantify the signal intensity of the green and red channel images per area. PECAM signal intensity was calculated by subtracting the red signal from the green and averaged for the sections from a single individual. *Nxn* $^{-/-}$ values were normalized to the average wild type value.